Deterministic Integration of hBN Emitter in Silicon Nitride Photonic Waveguide

Elshaari, Ali W.; Skalli, Anas; Gyger, Samuel; Nurizzo, Martin; Schweickert, Lucas; Esmaeil Zadeh, Iman; Svedendahl, Mikael; Steinhauer, Stephan; Zwiller, Val

DOI
10.1002/qute.202100032

Publication date
2021

Document Version
Final published version

Published in
Advanced Quantum Technologies

Citation (APA)
Elshaari, A. W., Skalli, A., Gyger, S., Nurizzo, M., Schweickert, L., Esmaeil Zadeh, I., Svedendahl, M., Steinhauer, S., & Zwiller, V. (2021). Deterministic Integration of hBN Emitter in Silicon Nitride Photonic Waveguide. *Advanced Quantum Technologies*, *4*(6), Article 2100032. https://doi.org/10.1002/qute.202100032

ADVANCED QUANTUM TECHNOLOGIES
www.advquantumtech.com

Deterministic Integration of hBN Emitter in Silicon Nitride Photonic Waveguide

Ali W. Elshaari, Anas Skalli, Samuel Gyger, Martin Nurizzo, Lucas Schweickert, Iman Esmaeil Zadeh, Mikael Svedendahl, Stephan Steinhauer, and Val Zwiller*

Hybrid integration provides an important avenue for incorporating atom-like solid-state single-photon emitters into photonic platforms that possess no optically-active transitions. Hexagonal boron nitride (hBN) is particularly interesting quantum emitter for hybrid integration, as it provides a route for room-temperature quantum photonic technologies, coupled with its robustness and straightforward activation. Despite the recent progress of integrating hBN emitters in photonic waveguides, a deterministic, site-controlled process remains elusive. Here, the integration of selected hBN emitter in silicon nitride waveguide is demonstrated. A small misalignment angle of 4° is shown between the emission-dipole orientation and the waveguide propagation direction. The integrated emitter maintains high single-photon purity despite subsequent encapsulation and nanofabrication steps, delivering quantum light with zero delay second order correlation function $g^{(2)}(0) = 0.1 \pm 0.05$. The results provide an important step toward deterministic, large scale, quantum photonic circuits at room temperature using atom-like single-photon emitters.

1. Introduction

In the last few years, there has been an increasing interest in hexagonal boron nitride (hBN) for optical quantum technologies after the discovery of single-photon emission at room temperature.[1–3] Such a property, coupled with straightforward generation of the defect, make hBN potentially viable for applications in quantum communication and sensing,[4] though the coherence of the emitted single-photons and its ramification on different target-applications is still to be investigated thoroughly, especially at short time-scales to explore fast exciton decoherence channels in the system.[5]. Defects in hBN can be viewed as "artificial atoms," having a ground and an excited state contained within the bandgap of the host material. The origin of the single-photon emission was recently attributed to the negatively charged defect $V_BC_N^-$ from carbon implantation.[6] The performance of the single-photon emitting defects in hBN have been studied extensively, they show high quantum efficiency and brightness,[7] in addition to being stable[1] and highly polarized both in emission and absorption.[8]

From a circuit integration point of view, hBN is a wide gap material making it suitable for a range of operating wavelengths. It has a refractive index of $n = 2.1$[9,10] in the visible range, comparable to other photonic materials such as aluminum nitride and silicon nitride (SiN), which simplifies the process of hybrid integration due to phase matching.[11] Moreover, second harmonic generation was also investigated in hBN,[10,12] such nonlinear response can enable novel applications of three-wave mixing in centro-symmetric photonic platforms through hybrid integration and exfoliation of hBN flakes. There has been extensive work into realizing photonic integrated circuits with hBN.[10] One approach is to directly form optical elements out of the hBN film,[13,14] which comes with the challenge of confining light exclusively in hBN due to its relatively small refractive index,[10] thus requiring under-etching of the substrate. The viability of under-etched large scale circuits for photonic application is still to be demonstrated, thus an alternative approach compatible with planar large scale photonic integrated circuits is needed. Non-deterministic hybrid integration of hBN in photonic circuits was recently demonstrated in aluminum nitride platform,[15] where hBN flakes were randomly dispersed on the photonic chip. Moreover, non-deterministic hybrid integration with suspended 1D

Prof. A. W. Elshaari, A. Skalli, S. Gyger, M. Nurizzo, Dr. L. Schweickert, Dr. M. Svedendahl, Dr. S. Steinhauer, Prof. V. Zwiller
Department of Applied Physics
Royal Institute of Technology
AlbaNova University Centre
Roslagstullsbacken 21, Stockholm 106 91, Sweden
E-mail: elshaari@kth.se
Prof. I. Esmaeil Zadeh
Optics Research Group
ImPhys Department
Faculty of Applied Sciences
TU Delft
Lorentzweg 1, Delft 2628 CJ, The Netherlands
A. Skalli, M. Nurizzo
Phelma, Physical engineering for photonics and microelectronics
Grenoble Institute of Technology
3 Parvis Louis Néel - CS 50257 - 38016 Grenoble Cedex 1, France
The ORCID identification number(s) for the author(s) of this article can be found under https://doi.org/10.1002/qute.202100032

DOI: 10.1002/qute.202100032

photonic crystal cavities was realized[16] through a wet transfer process of hBN to a SiN substrate. Pick and place technique for integrating hBN emitters to microcavity was demonstrated,[17] the strain induced from folding the hBN film on the resonator activates the hBN emitters. Position and spectral control of hBN single-photon emitters was also reported,[18] which opens exciting avenues for controlled integration of hBN emitters.

Several site-controlled integration methods were recently realized for QD-based single-photon emitters and defects in diamond.[19–23] Deterministic integration of hBN single-photon emitters is crucial for realizing complex photonic circuits with advanced functionalities,[11] especially with recent developments in chemical vapor deposition of hBN fabrication.[24] Here we deterministically integrate a high-purity hBN single-photon emitter in SiN photonic waveguide. Additionally, we measure close to ideal orientation of the dipole of the quantum emitter with respect to the waveguide cross section, which maximizes coupling between the dipole and the optical mode. **Figure 1**a shows an artistic representation of our device, it consists of an hBN single-photon emitter embedded in a SiN waveguide. In the following sections, the process of generating the single-photon defects in hBN and site-controlled process for waveguide integration is discussed.

2. Emitter Formation on SiO_2 and SiN Substrates

Figure 1b shows typical spectra of hBN emitters activated on two different substrates, SiO_2 and SiN, under illumination from 532 nm CW laser. Emitters annealed on SiN suffer from lower count rates and higher background fluorescence compared to the ones on SiO_2. As previously reported,[25] there is a four-fold increase in the fluorescence of annealed SiN at 1000°-1150° C compared to the as-deposited material. Moreover, the SiN photoluminescence emission peak blue shifts from around 800 nm for as-deposited substrate to ≈ 650 nm in annealed substrates above 1000° C, overlapping with the most frequent hBN emission wavelength in the statistical distribution of all measured emitters (see Supporting Information). This is attributed to reordering of atoms in the SiN film and creation of nano crystals, as previously investigated using TEM and GIXRD measurements.[25] Additionally, the high annealing temperatures introduce cracks in the SiN film which limits the size and complexity of fabricated photonic circuits. For the reasons above, we mainly focus on creating the quantum emitters on thermal SiO_2. Figure 1c shows a measured emission spectrum of the same hBN single-photon emitter at room temperature, and at 200 mK in 100 ms intervals, the emitter was activated on thermal SiO_2. The FWHM reduces from 3.75 nm at room temperature to 0.27 nm at 200 mK, which were extracted from fitting the emission peak under excitation from 50 μW continuous wave 532 nm laser. Moreover, we see that the emission is accompanied with spectral wandering at 200 mK. In Figure 1d we track the central emission wavelength as a function of time at 200 mK.

Despite observing reduction in the emission linewidth, the described spectral wandering of the emission peak on a millisecond time scale creates the perception of broadened emission due to averaging effects. hBN emitters on insulating substrates such as SiO_2 were reported to have larger spectral diffusion due to charge traps at the interface.[26] Furthermore, the two emission lines can be attributed to multiple excited states within a single hBN defect or complex of defects as reported in [27]. The possibility of several emitters closely positioned was ruled out through performing unfiltered, except for a long pass filter at 550 nm for laser rejection, second order correlation measurement as shown in Figure 1e. The result demonstrates the purity of the created defect as a single-photon emitter, where zero delay value is $g^{(2)}(0) = 0.30 \pm 0.06$. Figure 1f shows second order correlation measurement of the same emitter at 200 mK, the zero delay value is $g^{(2)}(0) = 0.33 \pm 0.03$. We notice the unfiltered zero delay value shows no significant change within experimental error between room temperature and 200 mK, despite the large reduction in linewidth. In all the reported measurements we perform no spatial filtering, for example through coupling to optical fibers,[28] thus all the signal from the hBN defect is focused using free space optics to two avalanche photo-diodes in a Hanbury–Brown and Twiss (HBT) configuration.

3. Site-Controlled Integration of Single-Photon Emitters in Waveguides

Following the previous results, the hBN emitters are first activated on a thermal SiO_2 film then the guiding layer of plasma enhanced chemical vapor deposition (PECVD) SiN is deposited on top of the emitters. This way no high-temperature annealing of SiN layer takes place, which can create a source of extra background fluorescence overlapping with our hBN single-photon emitters. In practice, depositing SiN on-top of pre-activated emitters severely reduced the quality and brightness of the emission, the cause is still under investigation. Thus, a protective thin intermediary layer of SiO_2 was deposited between the hBN flakes and the SiN photonic layer. Numerical simulations of coupling efficiency of hBN emitter to a 800 nm by 300 nm SiN waveguide as a function of the thickness of the intermediary SiO_2 layer is shown in **Figure 2**a. 40 nm thickness is selected, as it provides better encapsulation for larger hBN flakes, with acceptable coupling efficiency of ≈ 12% to the guided optical modes. Figure 2b shows the effect of the dipole orientation angle Φ in the encapsulated hBN on the coupling efficiency to the guided modes. It is crucial that the dipole of the hBN defect is aligned perpendicular to the waveguide propagation direction for maximum efficiency.

Figure 2c shows the fabrication process to integrate the hBN single-photon emitter in the waveguide deterministically. The substrate consists of a p-doped silicon wafer with 3 μm of thermal oxide, a marker field and a checker board pattern made of NbTiN are fabricated using electron-beam lithography, NbTiN sputtering, and lift-off (i). Drop casting of hBN solution (purchased from Graphene Supermarket) and thermal annealing to activate the quantum emitters (ii, iii). Deposition of 40 nm of PECVD SiO_2 and 300 nm of PECVD SiN (iv). The SiO_2 deposition was carried out using SiH_4:N_2O (710 sccm:425 sccm) chemistry at 800 mTorr and the SiN is deposited using SiH_4:NH_3 (800 sccm:16 sccm) chemistry at 650 mTorr. In both cases, the sample temperature was held constant at 300 °C, the RF power is 24 W at 13:56 MHz. Imaging of the emitters in the marker field, and imaging of a reference checker board pattern (v). The marker field is used for alignment of the emitters with respect to the

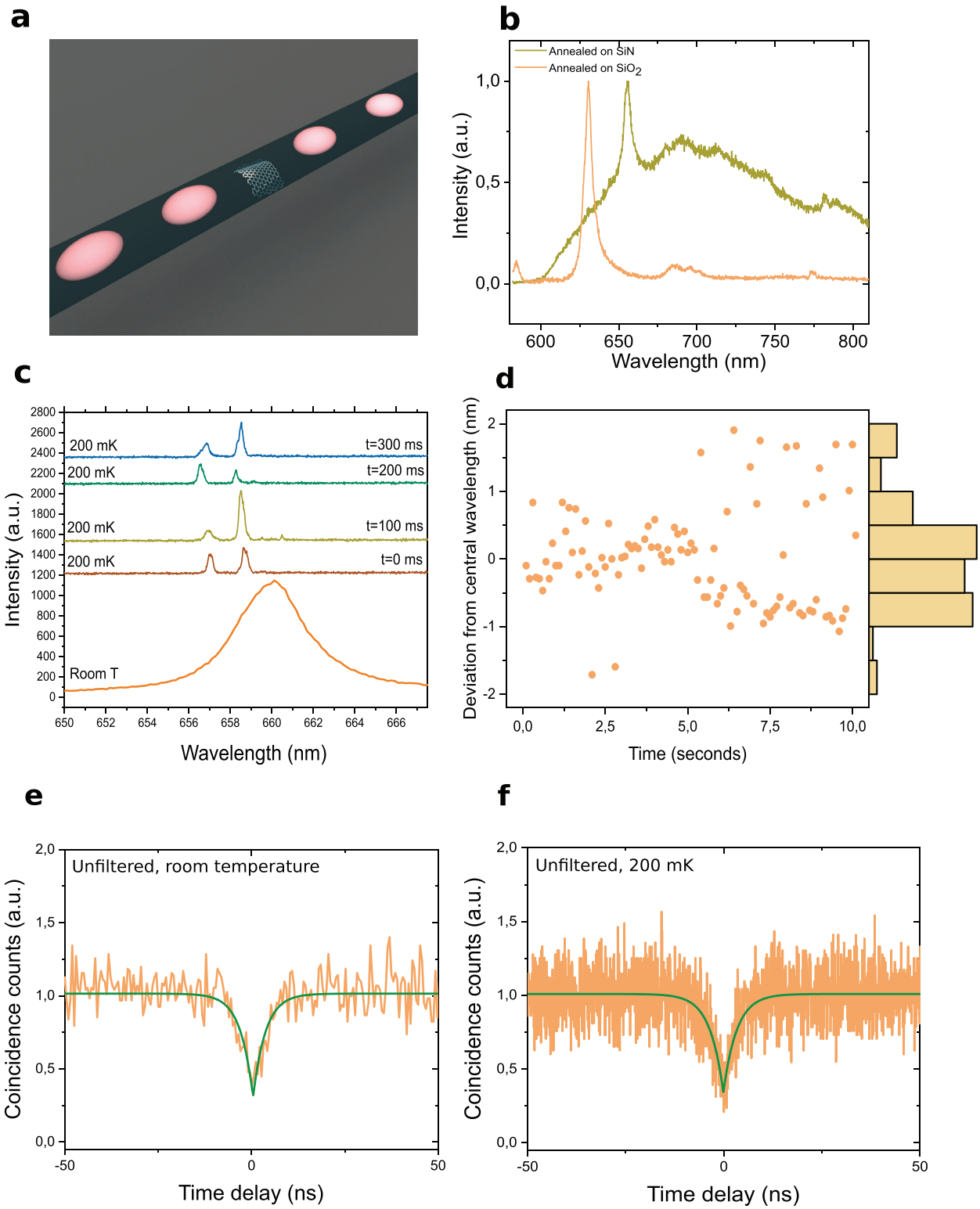

Figure 1. a) Artistic representation of a single-photon emitter in an hBN flake deterministically integrated in a SiN photonic waveguide. b) Photoluminescence of hBN emitters under excitation of 532 nm CW laser. The hBN flakes were dispensed on themal SiO_2 (orange) and SiN (green), then were annealed for 30 min at a temperature of 1100 ° C. c) Emission spectrum of a single hBN quantum emitter at room temperature , and 200 mK at different times, excited with 532 nm CW laser. d) Time trace of the center emission wavelength for the same emitter in (c) measured at 200 mK. e) Second order correlation function of the emitter in (c) at room temperature, no filtering was used for the emitter except for a long pass filter at 550 nm for laser rejection. The zero delay value with no filtering is $g^{(2)}(0) = 0.3 \pm 0.06$. f) Second order correlation measurement for the same emitter at 200 mK, the zero delay value with no filtering is $g^{(2)}(0) = 0.33 \pm 0.03$.

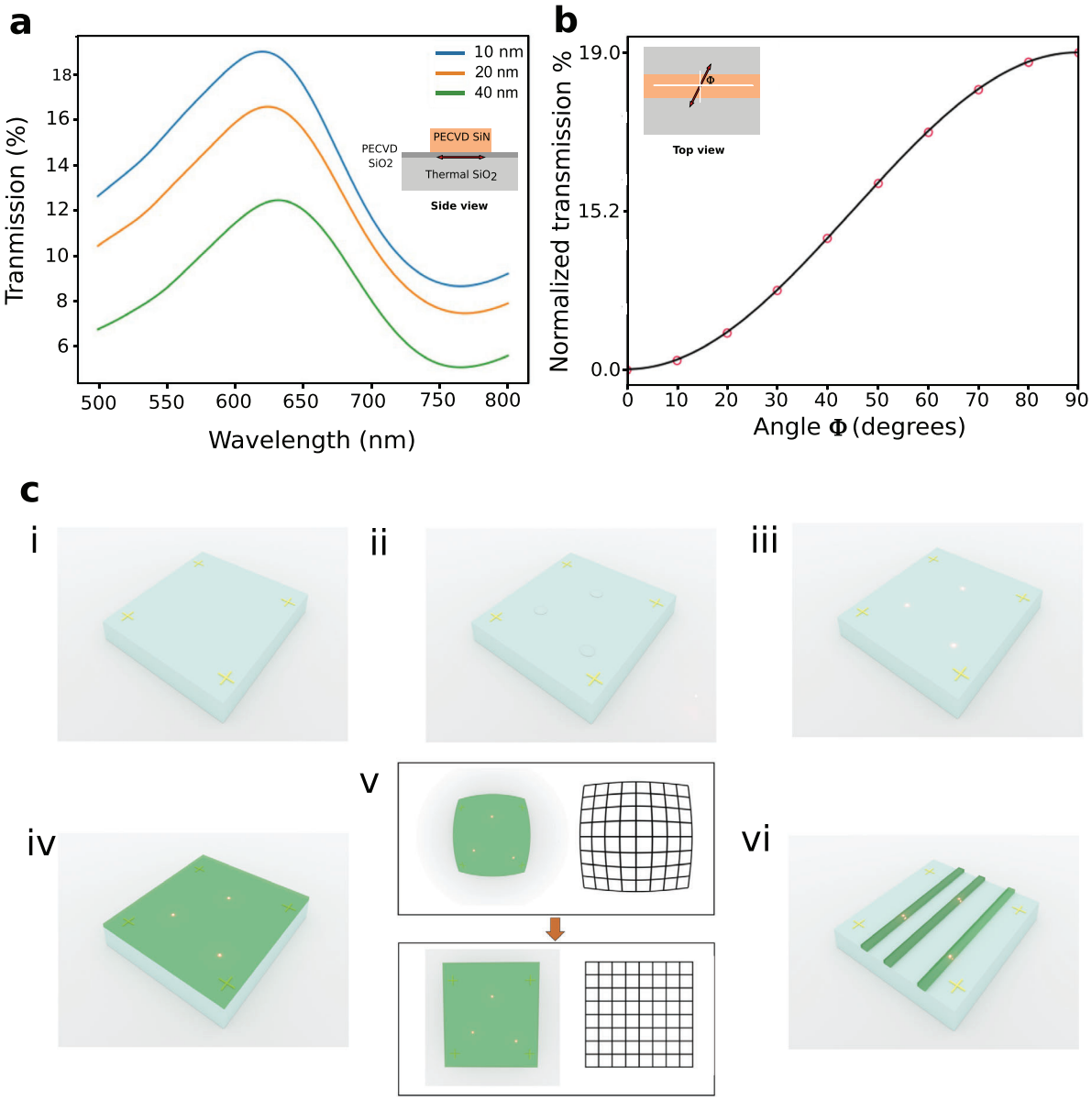

Figure 2. a) Finite difference time domain simulation of the total transmission of an hBN emitter integrated with a SiN photonic waveguide as a function of the protective SiO_2 layer thickness. b) Normalized coupling efficiency of hBN emitter to SiN photonic waveguide as a function of the orientation angle of the emission dipole with the waveguide propagation direction. c) Schematic of the fabrication process. i) Silicon wafer with 3 μm of SiO_2 and NbTiN marker field. ii) Drop casting of hBN flakes solution. iii) Activation of quantum emitters through annealing at 1100° C for 30 min. iv) Encapsulation of the quantum emitters in 40 nm PECVD SiO_2 and and 300 nm PECVD SiN. v) Imaging of the quantum emitters and correction of the barrel distortion through characterizing the nonlinear setup distortion using a fabricated checker board pattern on-chip. vi) Electron beam lithography and reactive ion etching to form the waveguide around the single-photon emitter.

subsequent lithography step, while the checker board pattern is used to correct for the barrel distortion in the imaging system. We correct for barrel distortion in the reference checker board pattern by finding the correct nonlinear transformation between the physical dimensions (from the design) and the collected image in our confocal microscopy setup. The generated numerical transformation is applied to the hBN emitter photoluminescence images to align them to the marker field with an error of less than 250 nm. Fabrication of photonic waveguides (vi). First, adhesion promoter (AR 300-80, All Resist) was applied to the substrate, followed by negative electronbeam resist ma-N 2403 (micro resist technology). After patterning of the waveguides using electron-beam lithography, reactive ion etching was performed using a mixture of CHF_3:CF_4:O_2 (30:5:5 sccm) under 100 W of RF power and temperature of 20° C.

4. Experimental Results

Figure 3a shows the experimental setup. It consists of a 532 nm CW pump laser which can be focused either through the

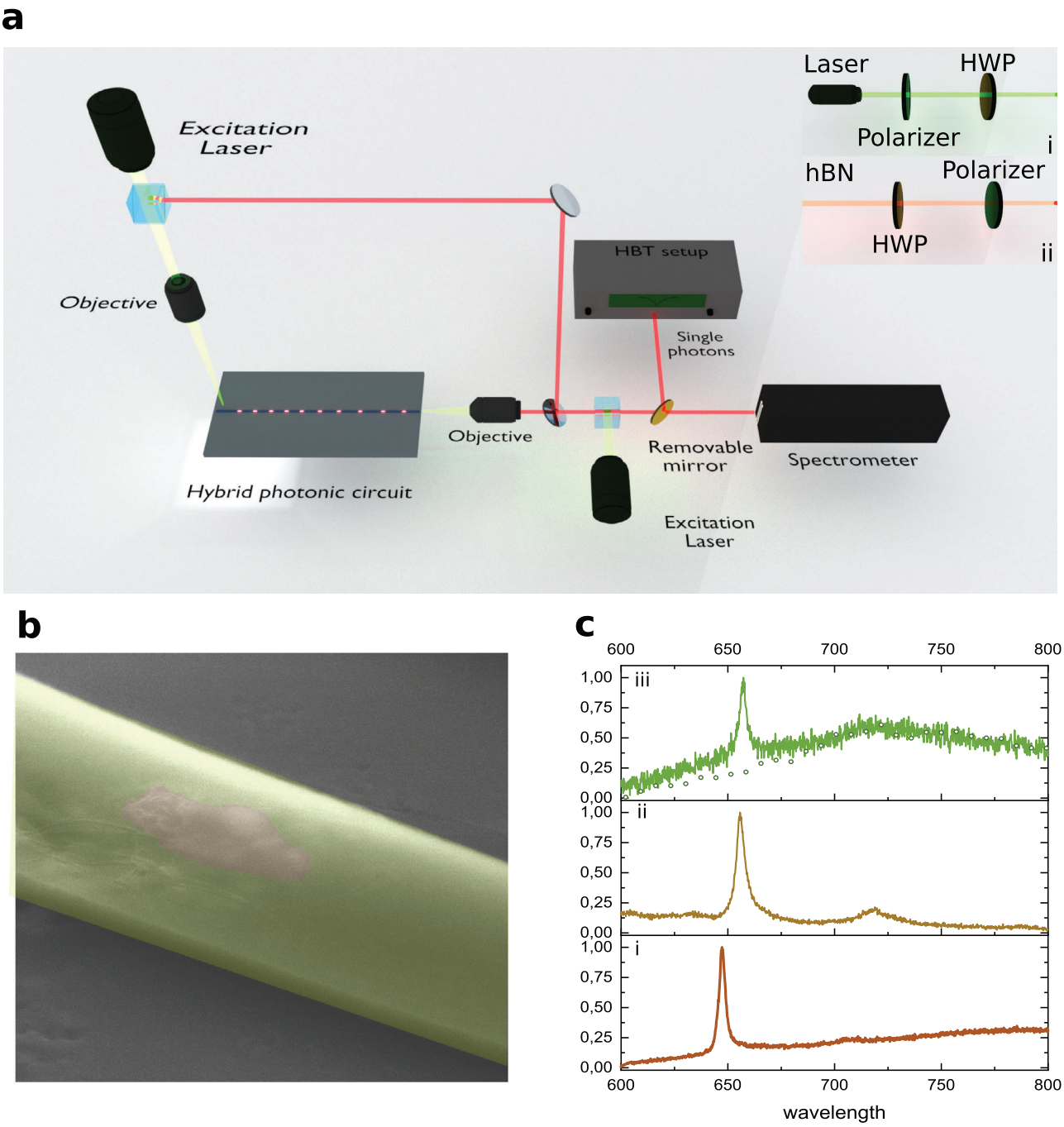

Figure 3. a) Experimental setup for testing the waveguide-integrated hBN single photo emitter, both top or through the waveguide laser excitation and photoluminescence collection can be selectively performed. The photoluminescence can be either coupled to a spectrometer for emission-spectrum measurement, or to a Hanbury Brown and Twiss setup with two avalanche photo diodes for second order correlation measurement. The inset shows absorption and emission polarization measurement to characterize the emission dipole direction of the hBN emitter with respect to the propagation direction of the waveguide. b) False color scanning electron microscope image of the SiN waveguide with deterministically integrated hBN single-photon emitter. c) Photoluminescence spectrum of an hBN emitter measured from the top i) before waveguide integration and ii) after waveguide integration. iii) Photoluminescence of the same emitter measured through the waveguide, the circles indicate the background photoluminescence of PECVD silicon nitride at room temperature. All the measurements in (c) were performed under CW laser excitation at wavelength of 532 nm.

waveguide using a 40× objective with NA=0.65, or from the top using a 10× objective with NA=0.28. The hBN emission signal can be selectively collected from each path using a removable mirror. The pump laser is filtered out through a 550 nm long pass filter, and the signal from the hBN is coupled to a 75 cm long spectrometer equipped with 150 and 1200 lines/mm gratings. Using a removable mirror, the signal from the hBN can be directed to an HBT setup for second order correlation measurement consisting of a 50/50 beam splitter and free-space coupled avalanche photo diodes.

In order to perform absorption polarization measurement (inset (i)), the laser is first polarized, then a half-wave-plate is used to rotate the pump polarization while the intensity of the hBN emission is recorded. Similarly for emission polarization measurement (inset (ii)), laser polarization is fixed while the signal from the hBN single-photon emitter is coupled to the spectrometer using a half-wave plate and a polarizer. Figure 3b shows false-color scanning electron microscope image of SiN waveguide integrated with hBN single-photon emitter, centered with high precision to the waveguide. Although, the hBN flakes are integrated at the interface between the SiN and SiO_2, their finite height[15] modifies the thickness of the deposited silicon nitride using PECVD (check Supporting Information for more SEM images of waveguide-integrated emitters). Figure 3c shows the emission collected from the hBN emitter in the waveguide. Inset (i): Top-excited and top-collected emission from the hBN defect encapsulated in the SiO_2 and SiN thin-films. The emission preserved similar qualities to emitters reported in Figure 1a, and elsewhere on SiO_2,[29] despite the encapsulation and the thermal treatment during the PECVD processes for both SiO_2 and SiN. Inset (ii): Same excitation and collection configuration after negative resist electronbeam lithography and reactive ion etching of the waveguide. We see an increase in the linewidth and a red-shift after the waveguide integration. A possible reason is the modification in both the local strain due to releasing of the tensile stress of SiN near the waveguide region due to etching,[30,31] and modification of the trapped charges in the hBN and SiO_2[26] interface from processing. Photoluminescence of the same emitter measured through the waveguide with top excitation (iii). The circles indicate the background photoluminescence of PECVD SiN at room temperature.[25] The large operating bandwidth of the waveguide allows for efficient coupling of photoluminescence from SiN which is superimposed on the hBN emission, reducing the overall signal to noise ratio. This is not a fundamental limit to the process, as other materials with larger transparency window and lower photoluminescence such as aluminum nitride,[32] silicon carbide,[33] and tantalum pentoxide,[34] can be used for the deterministic integration process we present here. For experimental data of more waveguide integrated emitters, and success probability of the site-controlled process, we refer the reader to the Supporting Information.

In our process, the emitters can be characterized thoroughly at every step of the integration enabling simultaneous control of the position and alignment of the waveguides with respect to the emitters position and their dipole orientation. **Figure 4**a shows emission and absorption polarization measurement of the same hBN emitter in Figure 3, the waveguide extends in 90°–270° direction. The emission dipole is aligned 86° from the propagation direction, only 4° error from the ideal 90° orientation. The misalignment between the absorption and emission dipole orientations is 20° as seen from Figure 4a. Generally, indirect transitions can occur in the emission process, which can result in misalignment between the absorption and emission dipole orientation.[35] Emitters with shorter wavelength, close to the laser excitation wavelength, have smaller angle of misalignment between absorption and emission dipole orientation as seen here. Figure 4b shows integrated counts of the hBN emitter versus excitation power, the emission is fitted with a simple three-level model,[36] using two fitting parameters I_∞ and P_{sat}. The signal (integrated hBN counts) to noise (background counts) ratio is extracted as a function of the excitation power as shown in Figure 4c. Excitation power of 20% P_{sat} maximizes the signal to noise ratio, this corresponds to 115 μW of excitation power. Figure 4d shows second order correlation measurement of the emitter excited with 115 μW of 532 nm CW pump. To minimize the signal from the SiN photoluminescence, a free-space band-bass 10 nm filter centered at the hBN emission peak is used. The zero-delay value of the measurement is $g^{(2)}(0) = 0.1 \pm 0.05$, proving the excellent purity of the integrated hBN single-photon emitter among state-of-art integrated layered emitters.[15,37,38]

Despite the promising presented results, the theoretical coupling efficiency of layered single photon emitters to photonic waveguides is far from the desired $\beta = 1$ for strong light–matter interaction.[39] One of the main reasons is the limitation of previous integration methods to placing the emitter on top of fabricated waveguides, then relying on evanescent coupling to the guided mode. Here, the presented fabrication method allows for encapsulation of the hBN emitter in the guiding, high index, material of the photonic waveguides. Thus through careful design of the photonic structure, and the material choice of the guiding layer, larger coupling efficiencies approaching unity are achievable. **Figure 5**a shows a hBN emitter encapsulated in an under-etched titanium dioxide waveguide with 1D photonic crystal mirror, providing broadband uni-directional coupling of the emitted photons to the forward direction. The waveguide has a width and height of 300 nm, the mirror consists of a fully-etched squares of length 200 nm, repeating every 450 nm. The broadband reflectively of the mirror and the large refractive index of titanium dioxide,[40] allows for reduction in the waveguide dimensions to support only the fundamental TE and TM modes. Moreover, titanium dioxide has a large bandgap with transparency window extending from near UV to IR,[40] covering the emission wavelength range of hBN. Figure 5b shows x–z and x–y cut for the power transmitted from the hBN dipole at 680 nm, where almost all the emitted photons are coupled to the fundamental TE mode. Figure 5c shows the forward coupling efficiency of the emitted photons from the hBN emitter to the fundamental TE mode for different wavelengths. The avoidance of resonant cavity structures, through the use of a single broadband mirror, results in high operation bandwidth of the device, the coupling efficiency is larger than 75% across more than 50 nm. Such a device has extraordinary potential for efficient single photon generation and non-linear optics at the single photon level.[39] Moreover, optical gating of hBN emitters can also be employed to increase the photoluminescence yield,[41] this becomes important to reach close to unity coupling between the emitter dipole and the traveling optical mode in the waveguide.

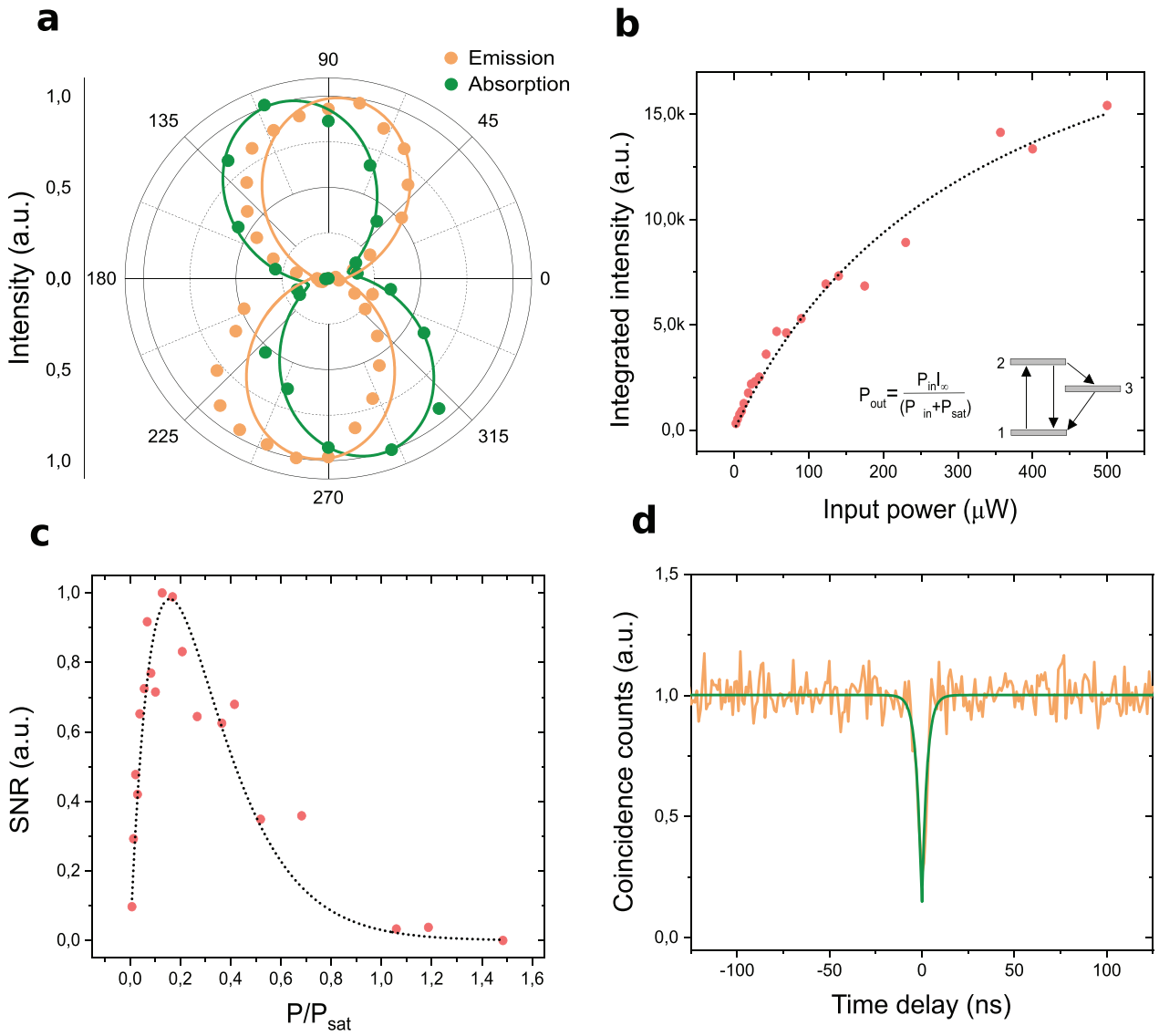

Figure 4. a) Dipole orientation characterization in absorption (green) and emission (orange), angle of 90° corresponds to the dipole emitter being perfectly perpindicular to the propagation direction. The waveguide extends in 90°–270° direction. b) Photoluminescence of the optical transition in the hBN emitter as a function of the excitation power, a simple three-level system model with one meta-stable state is used to fit the collected data. c) Signal to noise ratio of the photoluminescence as a function of the excitation power in units of P_{sat}. Top-measured Hanbury Brown and Twiss second order correlation of a waveguide integrated emitter with zero-delay value of $g^{(2)}(0) = 0.1 \pm 0.05$.

5. Conclusion

In conclusion, we presented a deterministic method of coupling hBN single-photon emitters to SiN photonic waveguides. The emitters were activated on thermal SiO_2, then encapsulated in a protective PECVD SiO_2 layer before depositing the SiN photonic-guiding layer. The waveguide integrated emitter shows high single-photon purity despite the fabrication steps with second order correlation function zero delay value $g^{(2)}(0) = 0.1 \pm 0.05$. Moreover, the emitter dipole orientation is aligned within 4° perpendicular to the propagation direction in the waveguide. Although theoretical coupling efficiency is far from the reported near unity coupling in other systems,[42] deterministic orientation of the dipole and higher confinement of the waveguides provides a route for stronger light-matter interaction in hybrid hBN quantum photonic circuits. The choice of SiN has the benefit of having a refractive index close to hBN, and provides a natural long-pass filter to reject the laser excitation at 532 nm.[20] The disadvantage is the significant photoluminescence near the hBN emission wavelength. Exploration of other photonic materials with larger transparency window and lower photoluminescence, in addition to employing resonant excitation[43] and conductive interfaces[26] can significantly improve the performance of integrated hBN emitters. Strain-tuning is another exciting avenue which can be used to engineer the optical properties of the emitter,[30] reconfigure the photonic circuit,[31] and align multiple-emitters within their linewidth. The presented deterministic integration method is compatible with previously

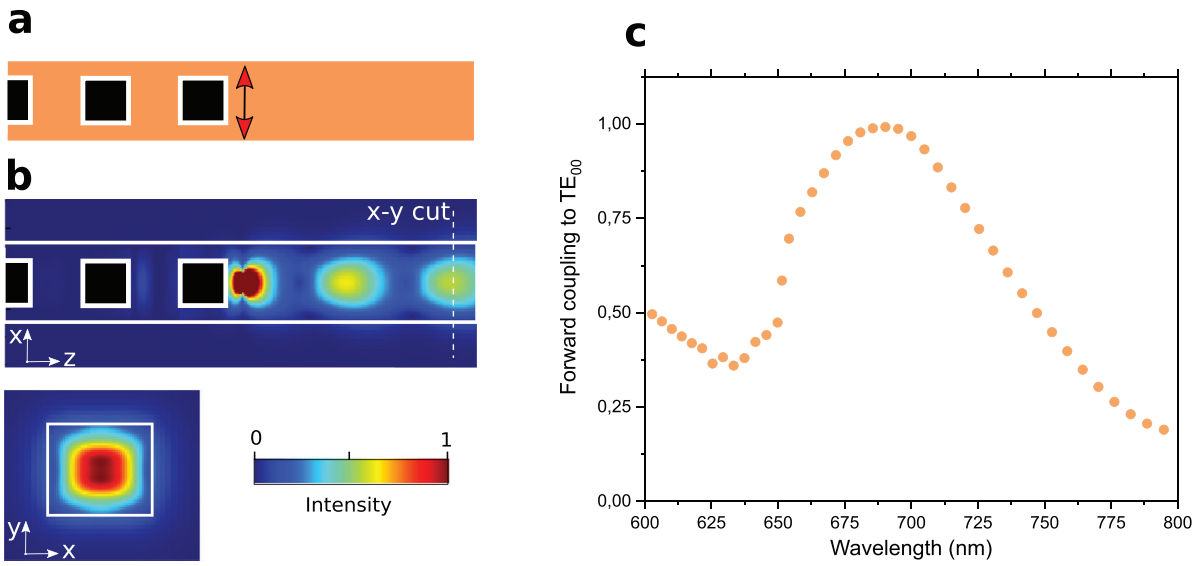

Figure 5. a) Schematic of hBN emitter embedded in titanium dioxide photonic waveguide with 1D broadband photonic crystal mirror. b) Intensity distribution of hBN emission at 680 nm wavelength. Almost all the emission is directed to the forward propagating fundamental TE mode of the waveguide. c) Forward transmission to the fundamental TE mode for different emission wavelengths of the hBN emitter.

reported controlled integration of superconducting single-photon detectors,[44] which provide means for generation and detection of non-classical light, all on-chip. Moreover, the versatility of the integration approach allows for demonstrating devices with near unity coupling efficiency to photonic modes through careful engineering of the photonic structure and the light-guiding material.

Supporting Information

Supporting Information is available from the Wiley Online Library or from the author.

Acknowledgements

A.W.E and A.S. contributed equally to the work. We acknowledge support from the Knut and Alice Wallenberg Foundation through the Wallenberg Centre for Quantum Technology (WACQT). A.W.E. acknowledges support from Vetenskapsrådet Starting Grant (Ref: 2016-03905). A.W.E. and I.E.Z. acknowledge support from the ATTRACT project funded by the EC under Grant Agreement 777222. S.S. acknowledges support from the Swedish Research Council (Vetenskapsrådet) Starting Grant (ref: 2019-04821).

Conflict of Interest

The authors declare no conflict of interest.

Data Availability Statement

The data supporting the findings of this study are available from the corresponding author on reasonable request.

Keywords

deterministic integration, hexagonal boron nitride, hBN emitters, hybrid quantum photonics, silicon nitride, single photons, waveguides

Received: March 3, 2021
Revised: April 14, 2021
Published online:

[1] T. T. Tran, K. Bray, M. J. Ford, M. Toth, I. Aharonovich, *Nat. Nanotechnol.* **2016**, *11*, 37.
[2] I. Aharonovich, D. Englund, M. Toth, *Nat. Photonics* **2016**, *10*, 631.
[3] T. T. Tran, C. Elbadawi, D. Totonjian, C. J. Lobo, G. Grosso, H. Moon, D. R. Englund, M. J. Ford, I. Aharonovich, M. Toth, *ACS Nano* **2016**, *10*, 7331.
[4] M. W. Doherty, N. B. Manson, P. Delaney, F. Jelezko, J. Wrachtrup, L. C. Hollenberg, *Phys. Rep.* **2013**, *528*, 1.
[5] B. Spokoyny, H. Utzat, H. Moon, G. Grosso, D. Englund, M. G. Bawendi, *J. Phys. Chem. Lett.* **2020**, *11*, 1330.
[6] N. Mendelson, D. Chugh, J. R. Reimers, T. S. Cheng, A. Gottscholl, H. Long, C. J. Mellor, A. Zettl, V. Dyakonov, P. H. Beton, S. V. Novikov, C. Jagadish, H. H. Tan, M. J. Ford, M. Toth, C. Bradac, I. Aharonovich, *Nat. Mater.* **2020**, *20*, 321.
[7] M. Nguyen, S. Kim, T. T. Tran, Z.-Q. Xu, M. Kianinia, M. Toth, I. Aharonovich, *Nanoscale* **2018**, *10*, 2267.
[8] A. L. Exarhos, D. A. Hopper, R. N. Patel, M. W. Doherty, L. C. Bassett, *Nat. Commun.* **2019**, *10*, 1.
[9] Y. Rah, Y. Jin, S. Kim, K. Yu, *Opt. Lett.* **2019**, *44*, 3797.
[10] J. D. Caldwell, I. Aharonovich, G. Cassabois, J. H. Edgar, B. Gil, D. Basov, *Nat. Rev. Mater.* **2019**, *4*, 552.
[11] A. W. Elshaari, W. Pernice, K. Srinivasan, O. Benson, V. Zwiller, *Nat. Photonics* **2020**, *14*, 285.
[12] S. Kim, J. E. Fröch, A. Gardner, C. Li, I. Aharonovich, A. S. Solntsev, *Opt. Lett.* **2019**, *44*, 5792.
[13] J. E. Fröch, Y. Hwang, S. Kim, I. Aharonovich, M. Toth, *Adv. Opt. Mater.* **2019**, *7*, 1801344.
[14] S. Kim, J. E. Fröch, J. Christian, M. Straw, J. Bishop, D. Totonjian, K. Watanabe, T. Taniguchi, M. Toth, I. Aharonovich, *Nat. Commun.* **2018**, *9*, 2623.

[15] S. Kim, N. M. H. Duong, M. Nguyen, T.-J. Lu, M. Kianinia, N. Mendelson, A. Solntsev, C. Bradac, D. R. Englund, I. Aharonovich, *Adv. Opt. Mater.* **2019**, *7*, 1901132.
[16] J. E. Fröch, S. Kim, N. Mendelson, M. Kianinia, M. Toth, I. Aharonovich, *ACS Nano* **2020**, *14*, 7085.
[17] N. V. Proscia, H. Jayakumar, X. Ge, G. Lopez-Morales, Z. Shotan, W. Zhou, C. A. Meriles, V. M. Menon, *Nanophotonics* **2020**, *9*, 2937.
[18] C. Fournier, A. Plaud, S. Roux, A. Pierret, M. Rosticher, K. Watanabe, T. Taniguchi, S. Buil, X. Quélin, J. Barjon, J.-P. Hermier, A. Delteil, *arXiv:2011.12224*, **2020**.
[19] M. Davanco, J. Liu, L. Sapienza, C.-Z. Zhang, J. V. D. M. Cardoso, V. Verma, R. Mirin, S. W. Nam, L. Liu, K. Srinivasan, *Nat. Commun.* **2017**, *8*, 889.
[20] A. W. Elshaari, I. Esmaeil Zadeh, A. Fognini, M. E. Reimer, D. Dalacu, P. J. Poole, V. Zwiller, K. D. Jöns, *Nat. Commun.* **2017**, *8*, 379.
[21] S. Aghaeimeibodi, B. Desiatov, J.-H. Kim, C.-M. Lee, M. A. Buyukkaya, A. Karasahin, C. J. Richardson, R. P. Leavitt, M. Lončar, E. Waks, *Appl. Phys. Lett.* **2018**, *113*, 221102.
[22] S. L. Mouradian, T. Schröder, C. B. Poitras, L. Li, J. Goldstein, E. H. Chen, M. Walsh, J. Cardenas, M. L. Markham, D. J. Twitchen, M. Lipson, D. Englund, *Phys. Rev. X* **2015**, *5*, 031009.
[23] N. H. Wan, T.-J. Lu, K. C. Chen, M. P. Walsh, M. E. Trusheim, L. De Santis, E. A. Bersin, I. B. Harris, S. L. Mouradian, I. R. Christen, E. S. Bielejec, D. Englund, *Nature* **2020**, *583*, 226.
[24] T.-A. Chen, C.-P. Chuu, C.-C. Tseng, C.-K. Wen, H.-S. P. Wong, S. Pan, R. Li, T.-A. Chao, W.-C. Chueh, Y. Zhang, Q. Fu, B. I. Yakobson, W.-H. Chang, L.-J. Li, *Nature* **2020**, *579*, 219.
[25] G. Scardera, T. Puzzer, I. Perez-Wurfl, G. Conibeer, *J. Cryst. Growth* **2008**, *310*, 3680.
[26] H. Akbari, W.-H. Lin, B. Vest, P. K. Jha, H. A. Atwater, *Phys. Rev. Appl.* **2021**, *15*, 014036.
[27] M. A. Feldman, C. E. Marvinney, A. A. Puretzky, B. J. Lawrie, *Optica* **2021**, *8*, 1.
[28] G. Grosso, H. Moon, B. Lienhard, S. Ali, D. K. Efetov, M. M. Furchi, P. Jarillo-Herrero, M. J. Ford, I. Aharonovich, D. Englund, *Nat. Commun.* **2017**, *8*, 705.
[29] C. Li, Z.-Q. Xu, N. Mendelson, M. Kianinia, M. Toth, I. Aharonovich, *Nanophotonics* **2019**, *8*, 2049.
[30] N. Mendelson, M. Doherty, M. Toth, I. Aharonovich, T. T. Tran, *Adv. Mater.* **2020**, *32*, 1908316.
[31] A. W. Elshaari, E. Büyüközer, I. E. Zadeh, T. Lettner, P. Zhao, E. Schöll, S. Gyger, M. E. Reimer, D. Dalacu, P. J. Poole, K. D. Jöns, V. Zwiller, *Nano Lett.* **2018**, *18*, 7969.
[32] T.-J. Lu, M. Fanto, H. Choi, P. Thomas, J. Steidle, S. Mouradian, W. Kong, D. Zhu, H. Moon, K. Berggren, J. Kim, M. Soltani, S. Preble, D. Englund, *Opt. Express* **2018**, *26*, 11147.
[33] D. M. Lukin, C. Dory, M. A. Guidry, K. Y. Yang, S. D. Mishra, R. Trivedi, M. Radulaski, S. Sun, D. Vercruysse, G. H. Ahn, J. Vučković, *Nat. Photonics* **2020**, *14*, 330.
[34] L. Splitthoff, M. A. Wolff, T. Grottke, C. Schuck, *Opt. Express* **2020**, *28*, 11921.
[35] N. R. Jungwirth, B. Calderon, Y. Ji, M. G. Spencer, M. E. Flatté, G. D. Fuchs, *Nano Lett.* **2016**, *16*, 6052.
[36] L. Novotny, B. Hecht, *Principles of Nano-Optics*, Cambridge University Press, Cambridge **2012**.
[37] F. Peyskens, C. Chakraborty, M. Muneeb, D. Van Thourhout, D. Englund, *Nat. Commun.* **2019**, *10*, 4435.
[38] C. Errando-Herranz, E. Schöll, R. Picard, M. Laini, S. Gyger, A. W. Elshaari, A. Branny, U. Wennberg, S. Barbat, T. Renaud, M. Sartison, M. Brotons-Gisbert, C. Bonato, B. D. Gerardot, V. Zwiller, K. D. Jöns, *ACS Photonics* **2021**, *8*, 1069.
[39] M. Arcari, I. Söllner, A. Javadi, S. Lindskov Hansen, S. Mahmoodian, J. Liu, H. Thyrrestrup, E. H. Lee, J. D. Song, S. Stobbe, P. Lodahl, *Phys. Rev. Lett.* **2014**, *113*, 093603.
[40] J. T. Choy, J. D. B. Bradley, P. B. Deotare, I. B. Burgess, C. C. Evans, E. Mazur, M. Lončar, *Opt. Lett.* **2012**, *37*, 539.
[41] P. Khatri, A. J. Ramsay, R. N. E. Malein, H. M. Chong, I. J. Luxmoore, *Nano Lett.* **2020**, *20*, 4256.
[42] M. Arcari, I. Söllner, A. Javadi, S. L. Hansen, S. Mahmoodian, J. Liu, H. Thyrrestrup, E. H. Lee, J. D. Song, S. Stobbe, P. Lodahl, *Phys. Rev. Lett.* **2014**, *113*, 093603.
[43] T. T. Tran, M. Kianinia, M. Nguyen, S. Kim, Z.-Q. Xu, A. Kubanek, M. Toth, I. Aharonovich, *ACS Photonics* **2018**, *5*, 295.
[44] R. Gourgues, I. E. Zadeh, A. W. Elshaari, G. Bulgarini, J. W. Los, J. Zichi, D. Dalacu, P. J. Poole, S. N. Dorenbos, V. Zwiller, *Opt. Express* **2019**, *27*, 3710.